UNIVERSITY *of York*

This is a repository copy of *Design of a Dual-Permanent-Magnet Vernier Machine to Replace Conventional Surface-Mounted Permanent Magnet Motor for Direct-Drive Industrial Turbine Application*.

White Rose Research Online URL for this paper:
https://eprints.whiterose.ac.uk/id/eprint/195697/

Version: Published Version

White Rose
university consortium
Universities of Leeds, Sheffield & York

eprints@whiterose.ac.uk
https://eprints.whiterose.ac.uk/

APPLIED RESEARCH

Design of a Dual-Permanent-Magnet Vernier Machine to Replace Conventional Surface-Mounted Permanent Magnet Motor for Direct-Drive Industrial Turbine Application

QIFANG LIN[1], XING ZHAO [ID]2, (Member, IEEE), FENGBIN CAI[3], QIANNAN WU[3], JIAPENG PANG[1], AND XINHUA GUO [ID]1

[1]College of Information Science and Engineering, Huaqiao University, Xiamen 361021, China
[2]Department of Electronic Engineering, University of York, YO10 5DD York, U.K.
[3]Xiamen Tungsten Company, Xiamen 361004, China

Corresponding author: Xing Zhao (xing.zhao@york.ac.uk)

ABSTRACT Surface-mounted permanent magnet motors (SMPMMs) have been widely used in industrial fields. However, when it comes to direct-drive low-speed large-torque fields, SMPMMs have several problems, such as lower slot filling factor, complicated fabrication, low efficiency, and bulky size. Recently, dual-permanent-magnet Vernier motors (DPMVMs) have been investigated due to their high torque density for low-speed direct-drive applications. However, so far, there is little research that demonstrates the application of the DPMVM for real industrial fields and quantitatively compares the performances of the DPMVM and the SMPMM. This paper studies the application of a DPMVM to the direct-drive industrial turbine as a replacement for conventional SMPMM. Rectangular and trapezoidal PMs are first applied to DPMVM in this paper. The performances of the DPMVM are quantitively compared with two typical SMPMMs. One is the design that has the same stator slots as the DPMVM, while the other has the same rotor pole pairs as the DPMVM. Economic costs are considered to form a thorough comparison between DPMVM and SMPMMs. It is revealed that with rectangular and trapezoidal PMs adopted in the DPMVM, the cost of PMs is significantly reduced with little sacrifice of performance. The efficiency of DPMVM is around 12% higher, and the material cost is reduced by 6.87% compared with the SMPMM.

INDEX TERMS Vernier PM machine, dual-PM, surface-mounted motor, comparative study, direct-drive, high efficiency.

I. INTRODUCTION

Machines are required to run at low speed with large output torque on many occasions, such as wind power generation, electric vessels, home appliances, etc. [1], [2], [3]. Usually, there are two methods to obtain large torque under low speed, one is to couple a high-speed machine with gearboxes, and the other is to design a motor at the desired operating

The associate editor coordinating the review of this manuscript and approving it for publication was Qinfen Lu [ID].

point and drive the load directly. For the first method, the mechanical gears introduce noise, require lubrication, and suffer substantial failure consequences [4]. For the second method, the absence of gearboxes eliminates the problems mentioned above. However, when directly driving the load, the machine usually becomes big and bulky.

A lot of effort is made to find machines with low speed and large torque density [5], [6], [7], [8]. Recently, Vernier permanent magnet machines (VPMs) have come into the view of researchers. The stator/rotor teeth of VPMs act as

TABLE 1. The main characteristics of the typical DPMVMs.

Reference	Winding Configuration	Stator PM configuration	Torque density	Thermal validation?
[19]	Fractional slot distributed winding	PMs in stator slots	28 kNm/m³	Not mentioned
[20]	Integer slot full pitch distributed winding	Halbach PMs in stator slots	23.1 kNm/m³	Not mentioned
[22]	Integer slot short pitch distributed winding	PMs in stator slots	34.5 kNm/m³	Not mentioned
[28]	Integer slot full pitch concentrated winding	Split stator teeth and Halbach PMs in stator teeth	12 kNm/m³	Not mentioned
[23]	Fractional slot short pitch distributed winding	PMs in left and right part of stator teeth alternatively	16.5 kNm/m³	Not mentioned
[29]	Fractional slot concentrated winding	Split stator teeth and Ferrite PM in stator teeth	Not presented	Not mentioned
[30]	Fractional slot concentrated winding	Split stator teeth and Ferrite PM in stator teeth	28 kNm/m³	Yes

the flux modulation pole. They function as the modulation ring in magnetic-geared machines [9], [10], [11], which means that only one layer of airgap is needed in the VPMs to realize the modulation effect. This makes the VPMs more compact. VPMs can be further divided into three categories, namely, stator-PM VM (has PMs only in stator part) [12], [13], [14], rotor-PM VM (has PMs only in rotor part) [15], [16], [17], [18], and dual-PM VM (has PMs in both stator and rotor) [19], [20], [21], [22], [23], [24]. For the former two machines, their torque density is not as high as dual-PM VM (DPMVM). This is because that PMs on both the stator and rotor of DPMVM contribute to output torque. In [20], DPMVM with Halbach PMs in stator slots and distributed winding was proposed and the torque density of it is 23.1 kN·m/m³ underrated condition. In [21], DPMVMs with distributed and concentrated winding were compared and it was found that DPMVMs with concentrated winding possess higher efficiency. The operation principle of DPMVM was illustrated clearly in [22] and the slot/pole combination equation is given. Recently, lots of DPMVMs with novel topologies are proposed, such as DPMVM with flux-concentrated PMs in stator teeth [25] and stator slots [26], DPMVM with hybrid teeth [27], and DPMVM with flux-concentrated PMs on both stator and rotor [28]. Although lots of DPMVMs with novel topologies have been proposed, their real application occasions have rarely been mentioned. In [29], DPMVM that adopts ferrite in stator teeth applied to the washing machine is investigated. The results show that the efficiency of the proposed DPMVM is higher than the conventional surface-mounted PM machine (SMPMM), however, the cost of the DPMVM is larger. And overall, the efficiency of the machine is relatively low and the temperature rise is not presented. In [30], DPMVM was investigated to apply in automatic guided vehicles, but the slot/pole combination was not investigated in detail. And there is no comparison between conventional PM machines. The main characteristics of the typical DPMVMs are listed in Table 1.

In this paper, a DPMVM with a two-split-teeth stator is designed to replace the conventional SMPMM in the industrial turbines. The performances of the initial SMPMM are exhibited first. Conclusions are drawn according to the FEM simulation and the experimental results. Further, in the third section, a DPMVM is designed following the design principles considering real application occasions and fair comparison. The topology and slot/pole combination of the DPMVM are carefully selected. Sensitivity analysis is used to simplify the optimization. Then all parameters are optimized. And a final design is obtained by changing the sector PMs to rectangular and trapezoidal shapes, considering the economic cost of PMs. Meanwhile, the DPMVM still keeps a better performance. In Section IV, the performances of the DPMVM are compared with two SMPMMs. One is the mentioned initial SMPMM which has the same stator slots as the DPMVM. The other is another SMPMM that has the same rotor poles as the DPMVM. Both the no-load and on-load performances of the three motors are investigated. Moreover, their material costs are also compared in detail. And the thermal field of the DPMVM is analyzed before making a prototype. An experimental study of the DPMVM prototype is conducted to validate the simulated results in Section V. Conclusions will be given in Section VI.

II. INITIAL SMPMM
A. SMPMM IN DIRECT-DRIVE INDUSTRIAL TURBINE SYSTEM
SMPMMs have been widely adopted in direct-drive industrial turbine applications. Fig. 1 shows one direct-drive industrial turbine product. In the direct-drive system, the gearbox is eliminated, and the blade of the turbine is connected to the rotor axial of the motor. Usually, the supply voltage of the motor is line-to-line 380 V (RMS).

Fig. 2 (a) shows the SMPMM used in a direct-drive industrial turbine system. The initial customer requirements, including the peripheral size, rated speed and power, rated
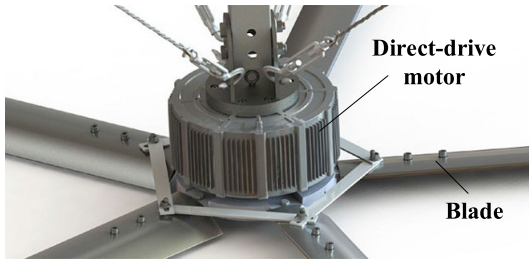
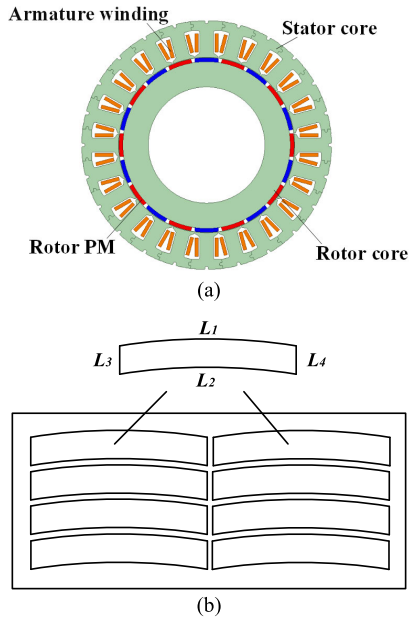**FIGURE 1.** Direct-drive motor in industrial turbine product.

FIGURE 2. SMPMM and its rotor PMs. (a) Topology of the SMPMM in direct-drive industrial turbine. (b) rotor PMs and rotor PMs on the blank.

TABLE 2. Customer requirements for initial motor for industrial turbine.

Requirements	Value
Outer diameter	300 mm
Stack length	50 mm
Wingding configuration	Concentrated
Rated voltage	~380 V
Rated speed	95 rpm
Temperature rise	≤88 K
Efficiency	≥76%
Rated torque	110 N • m
Rated power	1.1 kW

TABLE 3. Design parameters of the SMPMM.

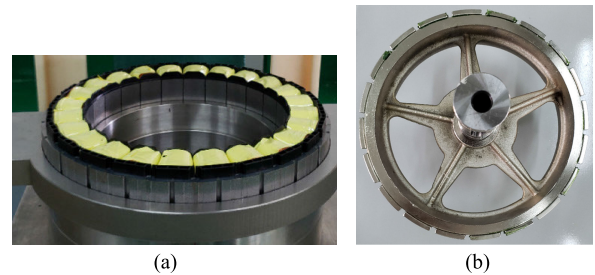| Items	Value
Stator slot	24
Air gap length	0.75 mm
Rated voltage	~380 V
Conductor number	262
Parallel branches	1
Rotor core type	Z45
Stator steel type	50WW470
PM type	N48SH
PM total weight	0.97 kg
PM remanence (T)	1.339, at 20°C

FIGURE 3. The prototype. (a) Stator. (b) Rotor.

TABLE 4. Experimental performances of the initial SMPMM.

Items	FEA Simulation	Experimental Result
Output torque/ N • m	123.2	110
Actual input current/A		2.3
Line-to-line Back-EMF/V	321.8	318
On-load voltage/V	343.3	357
Power factor	0.939	0.82
Copper loss/ W	326.2	327.8 (at 120°C)
Efficiency	77.4%	76%
Temperature rise/K	-	88

voltage, efficiency and temperature rise, are listed in Table 2. The detailed design parameters of this motor are presented in Table 3. It has 24 stator slots, 10 rotor pole pairs, and concentrated winding. The PMs of the SMPMM are mounted on the surface of the rotor, and their excitation modes are radially in and out alternatively. The enlarge view of the PMs and the PMs in the blank are shown in Fig. 2 (b). The shape of the PMs is specially designed to reduce the cost of the PMs. L_1 and L_2 are two arcs that have the same diameter, and L_3 and L_4 are parallel. According to the data provided by the manufacturer, the utilization rate of PM blank can be improved from 79.2% to 82.1%, and the manufacturing cost of PM can also be reduced.

B. SIMULATED AND EXPERIMENTAL PERFORMANCES OF THE SMPMM

In this part, the experimental performances of the SMPMM are exhibited. Fig. 3 shows the figures of the prototype, including the stator assembly and rotor core.

The experimental results of the SMPMM are listed in Table 4, and the experimental temperature-rise curve is

presented in Fig. 4. It can be noted that the temperature rise of the prototype is 88 K and the efficiency of the prototype is 76%. The temperature rise is measured by the thermistors set at the end of armature winding.

C. CONCLUSIONS

According to the simulation and experiment results presented in Part B, the following conclusions can be obtained:
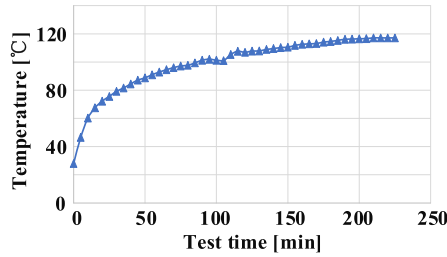
FIGURE 4. Experimental temperature rise curve of SMPMM.

- The error between the simulated torque and experimental torque is around 10%;
- The error between the back-EMF is 1.2%;
- The efficiency and temperature rise can just meet the performance requirements;
- The main loss of the SMPMM is the copper loss;

In order to improve the efficiency and decrease the temperature rise of the motor for the industrial turbine application, a dual-permanent-magnet motor (DPMVM) is designed to replace the initial SMPMM.

III. DESIGN AND OPTIMIZATION OF A DPMVM AS REPLACEMENT

A. BASIC PRINCIPLES FOR DESIGNING DPMVM

To have a fair comparative study, the basic design principles are listed as below:

- The material cost of the machine should not be higher than the initial SMPMM;
- The size of motor is kept the same as the initial SMPMM, including the outer diameter, airgap length, stack length;
- The rated speed, power, and output torque of the motor are kept unchanged;
- The temperature rise should be no more than required one, and the efficiency should be larger than 81.9%;
- The on-load line voltage of the machine should not be larger than 380 V;
- The slot number of the stator should be no larger than 24 for a large stator slot number will complicate the fabrication and reduce the overall slot filling factor;
- Concentrated winding configuration is considered.

Under these principles, the design process of the DPMVM is as follows:

- The topology and slot/pole combinations of DPMVMs are determined first;
- Sensitivity analysis is conducted to classify design parameters into different sensitivity level;
- Optimize the DPMVM based on the sensitivity analysis results.

B. SELECTION OF TOPOLOGY

The operation principle of DPMVMs is based on the flux modulation effect. Most of them have the same rotor structure, which consists of a PM-iron structure. The main
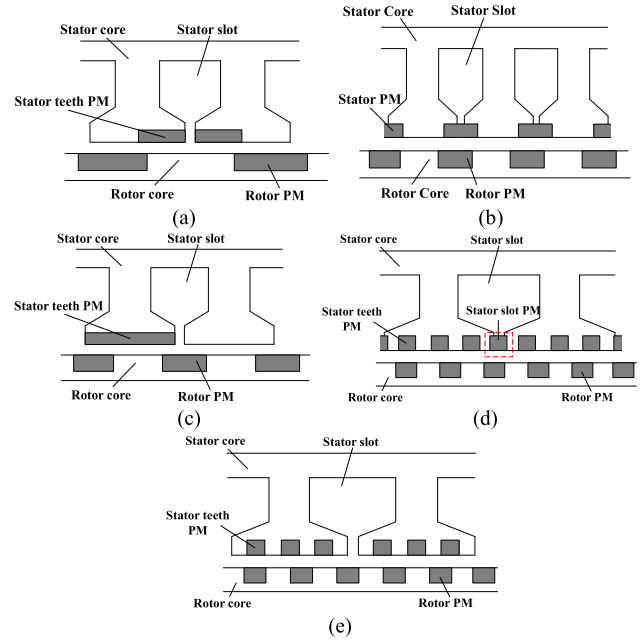

FIGURE 5. Typical configurations of the DPMVMs. (a) Model I. (b) Model II. (c) Model III. (d) Model IV. (e) Model V.

difference is the structure of the stator. According to present publications, the DPMVMs are divided into five types in this paper. Their topologies are shown in Fig. 5. For Model I shown in Fig. 5 (a), it has PMs magnetized in the same direction in stator slot openings. Each stator PM and its adjacent stator tooth form one pole pair. The stator tooth also acts as the modulator for the rotor PMs. Japanese researcher Ishizaki first proposed this kind of machine in [19]. It has also been investigated in [22]. The slot/pole combination of it follows

$$P_w = |P_r - N_s| \tag{1}$$

where P_w, P_r, and N_s are the pole pairs of armature winding, rotor pole pairs, and stator slots number, respectively. When considering concentrated armature winding, the stator slots number of this kind of motor cannot be reduced compared with conventional slot/pole combination. And most researches on this kind of machine focus on distributed armature winding.

For Model II, the characteristic of this structure is that the adjacent two stator teeth have PMs in different positions, and the alternat two stator teeth have the same PM position [23]. For Model III, it has PMs in alternative stator teeth. And the PMs cover the whole stator teeth [26]. All PMs have the same excitation direction. The slot/pole combinations of Model II and Model III follow Eq. (2). With the same number of P_r and P_w, this kind of structure has even larger N_s. And in existing published papers, most of these two configurations adopt distributed winding.

$$P_w = |P_r - N_s/2| \tag{2}$$

For Model IV, the stator of it is separated into several numbers of small teeth, n_{sp} (the number of small teeth in one big stator tooth), and PMs with the same excitation direction are located in both stator teeth and stator slots opening [21]. Model V has a similar configuration to Model IV. The difference is that the stator slot PMs in Model IV is removed in Model V. The slot/pole combination of Model IV and Model V follows

$$P_w = |P_r - n_{sp} \cdot N_s| \tag{3}$$

Model IV and Model V have been extensively investigated [21], [28], [29], [30], and it can significantly reduce the stator slots number by introducing n_{sp}. Considering concentrated winding, with the same P_r and P_w, the N_s of Model V can be smaller compared with Model I to Model III. Paper [29] demonstrated that the PMs in stator slot openings will introduce larger torque ripple and [30] exhibits that the small stator slot opening will lead to higher output torque.

According to the aforementioned analyses, when adopting concentrated armature winding, the topology of Model V is more suitable. By adopting this topology, higher rotor pole pairs can be achieved with even small stator slots.

C. SELECTION OF SLOT/POLE COMBINATION

For the topology determined in Section B, the slot/pole combinations of it have been investigated in [29], and it shows that the motor with 12 stator slots, n_{sp} equals to 2, P_r equals to 19 (12/2/19), has symmetric and sinusoidal back electromotive force (EMF). Moreover, it can produce higher torque density. Machine with 24/2/38 has been investigated in [30] for electric vehicle application. In this paper, the slot/pole combination of the motor is set as 24/2/38, which has the same stator slots as the initial SMPMM. The P_w is equal to 10 according to Eq. (3). The detailed reason for choosing 24/2/38 instead of 12/2/19 will be explained in Part F.

D. SENSITIVITY INVESTIGATION

The size parameters of the DPMVM are presented in Fig. 6. Here, "L" stands for length, "W" represents the width, and "A" represents the angle (the vertex of the angle is in the center of the inner circle). There are nine parameters in total. In the following parts, the parameters are divided into three classes based on the sensitivity analysis, namely, the strong-sensitive parameters, mild-sensitive parameters, and non-sensitive parameters. The step width of each parameter during the optimization process is determined according to the sensitivity analysis results.

The initial model of the DPMVM is carefully selected to avoid the saturation level of the stator and rotor core since the initial design is important for the accuracy of the sensitivity analysis. The flux density distribution of the initial model is shown in Fig. 7. The highest flux density of the iron core is around 1.7 T, and the saturation level of the core is 2.0 T.

The results of the sensitivity analysis are presented in Table 5. Here, S_E represents the sensitivity of the parameters
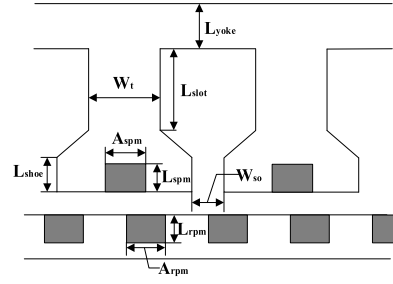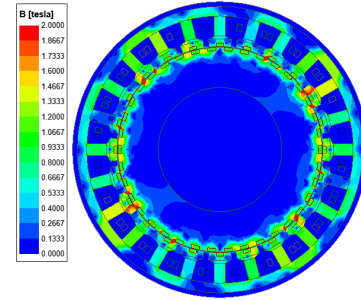

FIGURE 6. Size parameters of the DPMVM.

FIGURE 7. Flux density distribution of the initial design.

TABLE 5. Sensitivity analysis results.

Design parameter	Design objectives			Comprehensive sensitivity S_{total}
	S_E	S_{Tr}	S_{To}	
L_{yoke}	-0.008	4.118	-0.127	0.878
W_t	-0.021	-1.658	0.0718	0.369
L_{slot}	0.006	-6.061	-0.209	1.298
A_{spm}	0.056	-1.465	0.525	0.525
L_{spm}	0.003	-0.214	0.020	0.052
L_{shoe}	-0.004	2.866	-0.0462	0.593
W_{so}	-0.006	-0.436	-0.148	0.149
A_{rpm}	0.091	4.097	0.829	1.187
L_{rpm}	0.012	-0.235	0.118	0.099

to efficiency, S_{Tr} represents the sensitivity of the parameters to torque ripple, S_{To} is the sensitivity of the parameters to output torque, and the S_{total} represents the comprehensive sensitivity. The sensitivity level is calculated by

$$S(x_j) = \frac{x_{j0}}{O(x_0)} \cdot \frac{\partial O}{\partial x_j}\bigg|_{x_i=x_0} = \frac{\Delta O / O(x_0)}{\Delta x_j / x_{j0}} \tag{4}$$

where x_j is the parameter which is measured, and x_0 is the initial value of the parameter. $O(x_0)$ is the value of the objective when the parameter equals to x_0. And the comprehensive sensitivity value is obtained by

$$S_{total} = w_E |S_E| + w_{Tr} |S_{Tr}| + w_{To} |S_{To}| \tag{5}$$

where w_E equals to 0.4, w_{Tr} equals to 0.2, w_{To} equals to 0.4, are the weight coefficients and the subtotal of these three parameters is equal to 1.

TABLE 6. Classification of each parameter.

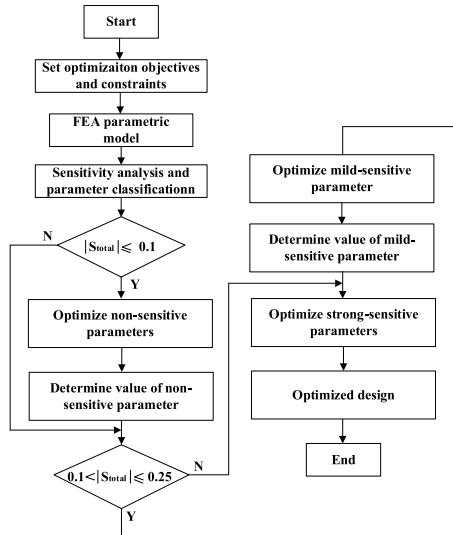| Groups	Parameters
Non-sensitive	L_{rpm}, L_{spm}
Mild-sensitive	W_{so}
Strong-sensitive	L_{yoke}, W_t, L_{slot}, A_{spm}, L_{shoe}, A_{rpm}

FIGURE 8. Flow chart of the optimization process.

Based on the results of the S_{total}, the sensitivity levels of the parameters are divided into three levels

$$\begin{cases} S_{total} \leq 0.1, & non\text{-}sensitive \\ 0.1 < S_{total} \leq 0.25, & mild\text{-}sensitive \\ S_{total} > 0.25, & strong\text{-}sensitive \end{cases}$$

The classification and the step width of each parameter are presented in Table 6.

E. OPTIMIZATION

According to the sensitivity analysis results, the DPMVM is further optimized. The flow chart of the optimization process is shown in Fig. 8. Non-sensitive parameters will be optimized firstly, then mild-sensitive and strong-sensitive parameters will be optimized. The objective function can be written as

$$O(x) = \{\min(T_r), \max(T_o, \eta)\} \quad (6)$$

The non-sensitive parameters, L_{rpm} and L_{spm}, are optimized first. The effect of these two parameters on the objectives is illustrated in Fig. 9. Fig. 9 (a) shows that the output torque increases as the increase of L_{rpm} fast, and then the increasing rate decrease after 3mm. And the same to L_{spm}. From 2-3 mm, output torque increases as L_{spm}, and after 3 mm, the output torque tends to decrease. From Fig. 9 (b), it can be noted that the trend of L_{rpm} and L_{spm} to efficiency is
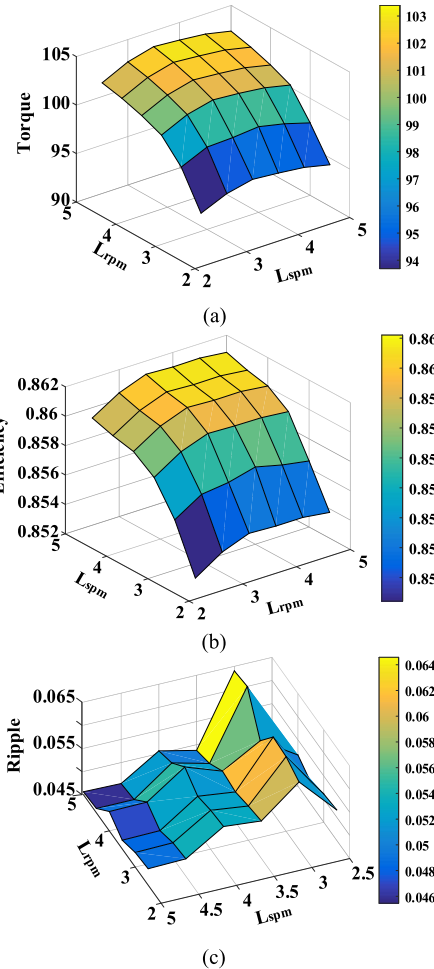

FIGURE 9. Optimization objectives versus L_{rpm} and L_{spm}. (a) Output torque versus L_{rpm} and L_{spm}. (b) Efficiency versus L_{rpm} and L_{spm}. (c) Torque ripple versus L_{rpm} and L_{spm}.

similar to that of torque. For torque ripple shown in Fig. 9 (c), it can be found that the torque ripple increases rapidly when L_{spm} is smaller between 3 and 3.5 mm. For L_{rpm}, the torque ripple fluctuates as the changing of L_{rpm}. However, when L_{spm} is smaller than 3.5 mm, the ripple is not high on the whole when the L_{rpm} is varying. Considering three objectives, the values of the L_{rpm} and L_{spm} are set as 5 mm and 3.5 mm to obtain high output torque and efficiency. Meanwhile, keeping an acceptable torque ripple.

The mild-sensitive parameter W_{st} is optimized, based on the determined L_{rpm} and L_{spm}. Fig. 10 shows the variation of the objectives with W_{st}. From Fig. 10 (a), it can be found that the output torque is reduced as the increase of W_{st}. And the efficiency is slightly increased as W_{st} before 4.8 mm. After this point, the efficiency is slightly decreased, and from 6 mm, it decreases obviously. For torque ripple, it can be noted that when W_{st} is larger than 10.4 mm, the torque ripple increases rapidly. It is acceptable to choose W_{st} between 4-6mm. Considering the stator winding embedding process, the W_{st} should be slightly bigger to facilitate the processing. Thus, W_{st} is set as 5.6 mm for further optimization.
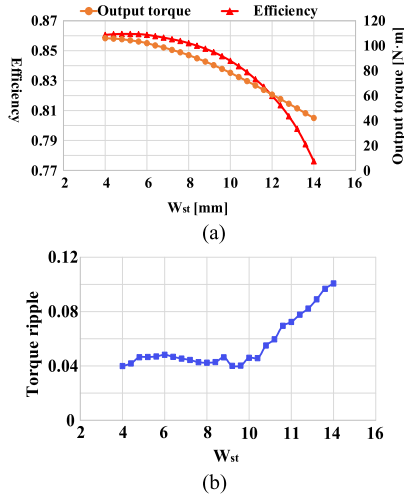
FIGURE 10. Optimization objectives versus W_{st}. (a) Output torque and efficiency versus W_{st}. (b) Torque ripple versus W_{st}.
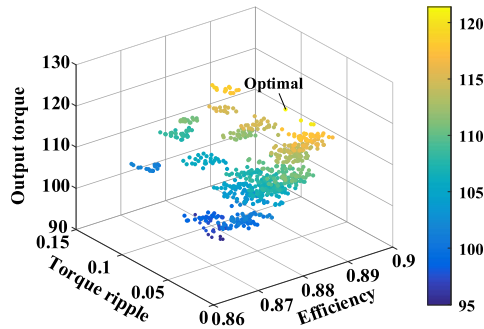

FIGURE 11. Distribution of the objectives during the optimization process.

The results during the optimization process of strong-sensitive parameters are shown in Fig. 11. With the appropriate design of the parametric model, the changing of the strong-sensitive parameters will not affect the values of non-sensitive and mild-sensitive parameters. An optimal point with maximum output torque, efficiency, and acceptable torque ripple is selected for further analysis. Its detailed performances will be investigated in the following sections.

F. FINAL DESIGN OF DPMVM CONSIDERING THE COST

The configuration of the DPMVM after optimization is shown in Fig. 12. From the large-scale view, it can be observed that the shape of the stator PM (SPM) and the rotor PM (RPM) is sector. According to the data provided by the manufacturer, the utilization rate of the blank of sector shape PM is only 79.2%. However, the utilization rate of the rectangular PM is 82.6%. Moreover, the processing cost of sector PM per kilogram is more than twice that of rectangular PM. Thus, considering the utilization rate and processing cost, the shape of the SPMs and RPMs is modified as a rectangular shape. By doing this, a little performance is sacrificed, but the price is greatly reduced. Table 7 shows the
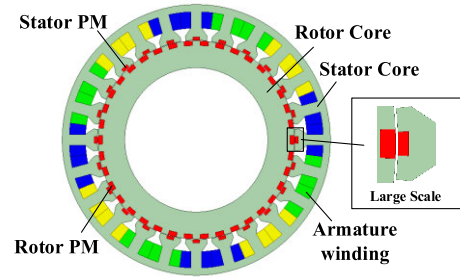

FIGURE 12. Optimized configuration of the DPMVM.

TABLE 7. Performances of the optimized motor and final design.

Items	Optimized motor	Final design
T_o	122.7	119.5
T_r	5.4%	6.7%
Core loss	23	19.6
Efficiency	88	88.4
PM processing cost (USD)	108.7	86.5

performances of the optimized motor and the modified final design. It can be observed that the torque ripple of the motor is slightly increased by 1.3%. The output torque is reduced by 3.2 Nm. The ultimate efficiency of the modified motor is increased by 0.4% due to the decrease in core loss. The PM cost of the final design is reduced by 17.7%. We can find that the change of shape of stator and rotor PMs has little effect on the performance of the motor. This is because as the stator and rotor pole pairs increase, the shape of the stator and rotor PMs are already near rectangular. This is also the reason why the slot/pole combination 12-2-19 is not selected in this paper. For the 12-2-19 motor, when changing the stator and rotor shape to rectangular, the stator part and rotor parts may face intersections in the airgap because the smallest air gap length becomes lower than 0.4 mm. Moreover, this distortion of air length will lead to a larger torque ripple. Thus, the slot/pole combination of 24-2-38 is selected.

IV. COMPARATIVE STUDY AND THERMAL FIELD VALIDATION

In this section, the electromagnetic performances of the DPMVM will be compared with two SMPMMs, as well as the material cost of the three motors. One SMPMM is the initial SMPMM (SMPMM I) in Section II. It has the same number of stator slots and winding pole pairs as the DPMVM. The other SMPMM has the same rotor pole pairs as the DPMVM and 72 stator slots (72SMPMM). The configuration of the 72SMPMM is shown in Fig. 13. 72SMPMM is optimized under the same objectives as DPMVM. The material types and critical design parameters, like air gap length, peripheral size, rated voltage, rated speed, and rated power of the 72SMPMM, are kept the same as the other two motors to have a fair comparison. Moreover, the PM of 72SMPMM is also designed as a trapezoidal shape to reduce the cost.
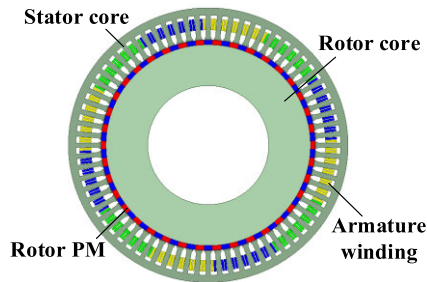
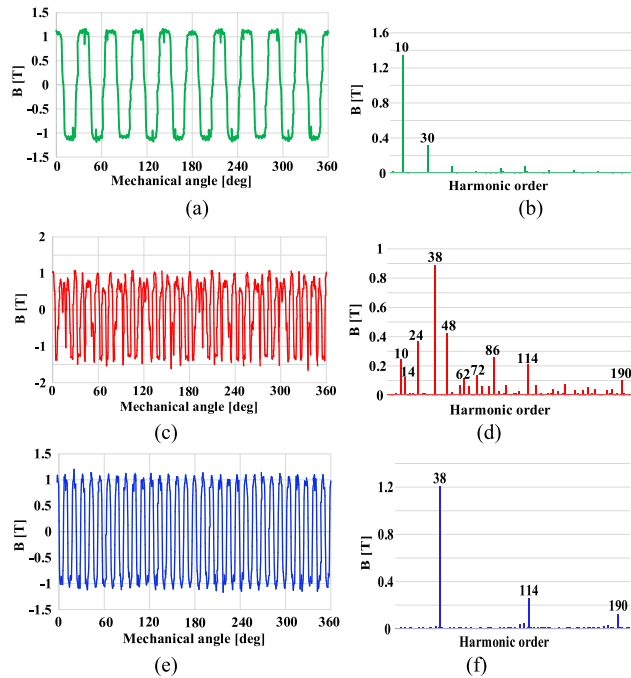**FIGURE 13.** The structure of SMPMM with 72 stator slots(72SMPMM).

FIGURE 14. Airgap flux density waveforms of the three motors and their harmonic components. (a) Flux density waveform of 24SMPMM. (b) Harmonic components of 24SMPMM. (c) Flux density waveform of DPMVM. (d) Harmonic components of D∈M. (e) Flux density waveform of 72SMPMM. (f) Harmonic components of 72SMPMM.

A. OPEN-CIRCUIT PERFORMANCES
The open-circuit performances, including the airgap flux density, back-EMF, and cogging torque of the three motors, are investigated in this part.

1) FLUX DENSITY DISTRIBUTION
Fig. 14 illustrates the airgap flux density and the harmonic analysis results of the three motors. It can be found that there are abundant harmonics in the airgap of DPMVM compared with two conventional SMPMMs. As it analyzed in [21], the effective harmonic components of DPMVM includes 10, 24, 38, 48, 72, 114, 190. For 24SMPMM and 72SMPMM, the effective harmonic orders are equal to the winding pole pair, which are 10 and 38, respectively.

2) BACK-EMF AND COGGING TORQUE
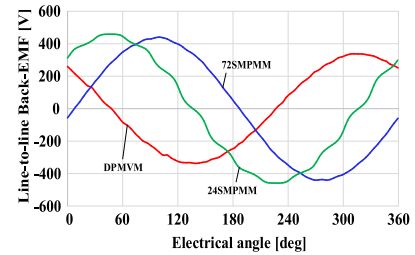The waveforms of the back-EMF of the winding are depicted in Fig. 15. The RMS value, THD value, and the peak-to-peak

FIGURE 15. Line-to-Line back-EMF of three motors.

TABLE 8. Back-EMF and cogging torque of the three motors.

Items	24SMPMM	DPMVM	72SMPMM
Back-EMF	321.8	237.7	309.4
Normalized back-EMF	1.00	1.63	1.02
THD	3.75%	0.89%	1.44%
Cogging torque	2.5 N·m	6.1 N·m	2.1 N·m

TABLE 9. On-load performances of the three motors.

Items	24SMPMM	DPMVM	72SMPMM
Output torque/N·m	123.2	119.5	119.4
Torque ripple/%	5.6	6.7	3.7
Current/A	2.3	2.97	2.32
Copper loss/W	326.2	113.8	223.6
Core loss/W	8.7	19.6	17
Current density/(A/mm²)	2.3	2.97	2.32
Thermal Load/(A²/(cm·mm²))	2277	794.5	1965.3
Fractional loss/W		22	
Efficiency/%	77.4	88.4	81.9
Power factor	0.939	0.68	0.989

of the cogging torque of the three motors are exhibited in Table 8. It can be noted that the THD value of the DPMVM is the lowest one among the three motors. Moreover, the normalized back-EMF of the DPMVM is the highest. The cogging torque of the DPMVM is the highest.

B. ON-LOAD PERFORMANCES
Based on the FEA simulation and the experimental results of the initial 24SMPMM in Section II, Part B, the output torque of the rest two motors is designed around 120 N·m. The on-load performances of the three machines are presented in Table 9.

1) TORQUE
The simulated output torque is designed near 120 N·m to guarantee a reasonable result. The torque ripple of the DPMVM is highest among three machines, but it is acceptable for industrial turbine application.

2) LOSSES
The copper losses of the three motors are estimated by the same method. It can be noted that the copper loss of DPMVM is around one-third of the 24SMPMM and one-half of the 72SMPMM. Moreover, it can also be found that the copper loss is the main loss of the three motors, which means the

TABLE 10. Material cost of the three motors.

Items	24SMPMM	DPMVM	72SMPMM
Copper weight/kg	4.42	4.08	3.0
Copper cost/ USD	52.6	48.6	35.7
PM weight/kg	0.97	0.96	1.48
PM material cost/USD	87.9	86.5	133.3
PM processing cost/USD	12.9	6.3	9.6
Silicon cost/ USD	35.8	34.8	32.8
Total/ USD	189.2	176.2	211.4

copper loss is the primary source of the heat. From the experimental results of 24SMPMM in section II, it can be seen that the stable operating temperature of the 24SMPMM is near 120 ° under a thermal load of 2277 $(A^2/(cm·mm^2))$. Furthermore, the thermal load of the DPMVM is around one-third of the 24SMPMM, which tells that the temperature rise of the DPMVM should be less than the 24SMPMM. The core loss of the DPMVM is the highest among the three motors. This is because the core loss is proportional to the frequency and the amplitude of flux density. The frequency of DPMVM is 3.8 times that of 24SMPMM. And the total effective flux density of DPMVM is also higher than the two SMPMMs. Thus, the core loss of DPMVM is the highest one among the three motors.

3) EFFICIENCY

The estimated efficiency of the DPMVM is 88.5%, which is the highest one among the three motors. And that of the 24SMPMM is the lowest one.

4) POWER FACTOR

The power factor of the DPMVM is the lowest one among three motors. But this value is still acceptable and better than regular DPMVM. Moreover, for industrial turbine application, the power factor requirement of motor is not so high compared with servo motor.

C. MATERIAL COST

For the real industrial application, it is necessary to take the cost of the motor into consideration. Therefore, the cost of the three motors under the same output power is compared in this part.

It can be seen from Table 10 that the cost of DPMVM is the lowest, which is 6.87% cheaper than 24SMPMM and 16.65% cheaper than 72SMPMM. It does not seem much with a 6.87% reduction, but it will significantly benefit mass production. Moreover, the efficiency of the DPMVM is also higher than the two SMPMMs, and more energy will be saved on the customer side, and this will also bring benefits.

Through the comparative study, it can be concluded that the DPMVM has higher efficiency and lower cost than the three motors. Thus, the DPMVM is selected to craft a prototype. Its thermal condition will be simulated before fabrication.
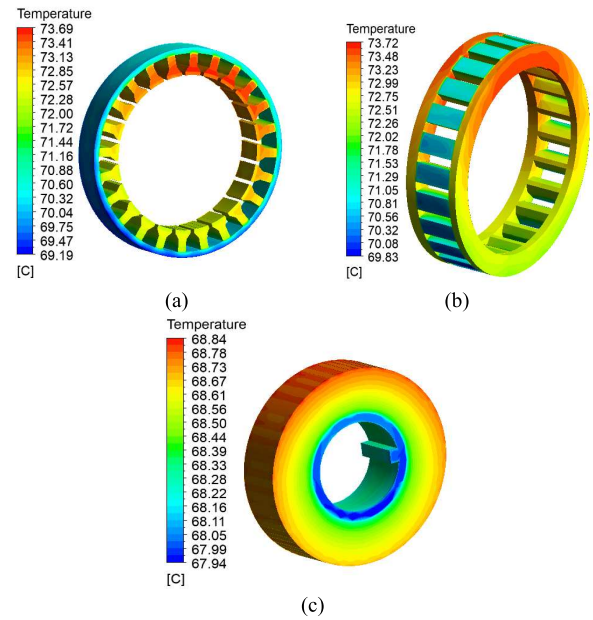

FIGURE 16. The thermal distribution of the DPMVM. (a) Stator core and stator PMs. (b) Armature winding. (c) Rotor core and rotor PM.
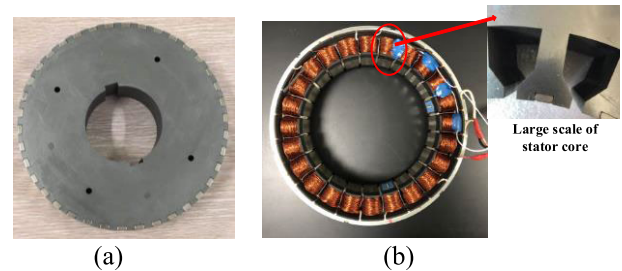

Large scale of stator core

FIGURE 17. The prototype of the proposed DPMM. (a) Rotor assembly. (b) Stator assembly.

D. THERMAL FIELD VALIDATION

To verify the feasibility of the DPMVM, its thermal field is analyzed. The environment temperature is assumed as 25 °C. Fig. 16 shows the temperature distributions of each part of the DPMVM. It can be found that the highest temperature is at the end of armature winding, which is 73.72 °C. The average temperature of the armature winding is 72.9 °C. This indicates the simulated temperature rise of the DPMVM is only 47.9 K. And the required temperature rise is no more than 80 K. Thus, the simulated temperature rise of the DPMVM fulfills the requirement.

V. EXPERIMENTAL VALIDATION

A prototype of the DPMVM is fabricated to verify the accuracy of the simulated results and the feasibility of the DPMVM for the industrial turbine. Fig. 17 shows the rotor and stator assemblies. The thermistors are set at the end of the armature winding. The test platform is shown in Fig. 18. A power analyzer is used to detect input power, output power, and the power factor of the motor.
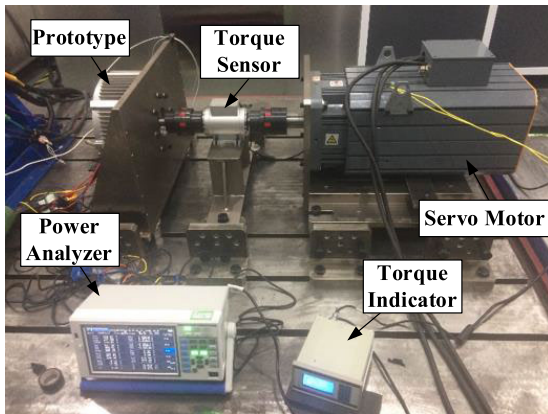
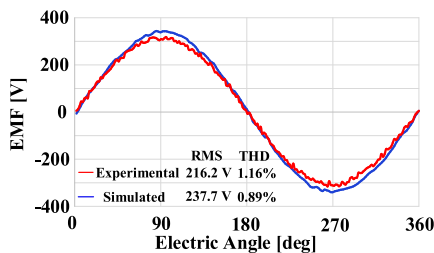**FIGURE 18.** The experiment platform of the proposed DPMM.

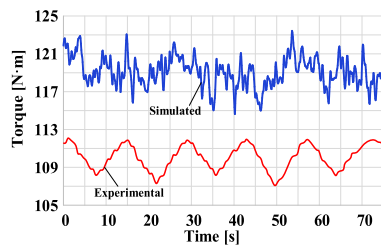**FIGURE 19.** The line-to-line back EMF of the proposed DPMM.

FIGURE 20. The simulated and experimental output torque of the DPMVM.

Fig. 19 depicts the simulated and experimental back-EMF waveform of the DPMVM and the corresponding THD value. The error between simulated and experimental RMS value is around 9.08%. This error may be induced by the simulation error and manufacturing error. And the simulated and experimental THD value of back-EMF is close.

The rated output torque of the DPMVM is shown in Fig. 20. It can be noted that the experimental output torque is 110.6 N·m which is 7.4% lower than the simulated one. The experimental torque ripple 4.3%, which is also lower than the simulated one. This is because the torque ripple of the DPMVM is related to the load. When the inertia of the opposite traction motor is large, the torque ripple detected by the torque sensor will be reduced as well.

The phase voltage and current waveform measured by the power analyzer is shown in Fig. 21. The power factor obtained from this figure is 0.6 and the simulated one is 0.68, which is very close. The experimental efficiency of the prototype
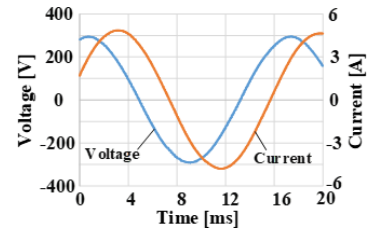

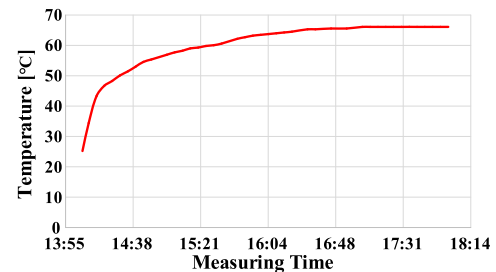**FIGURE 21.** The experimental on-load voltage and current of Phase A.

FIGURE 22. The temperature rise curve.

measured by the power analyzer is 88%. This result is close to the simulated one.

The temperature rise curve of the DPMVM is shown in Fig. 22. It is measured by the thermistor KTY-84 set at the end of the armature winding. It can be noted that the ultimate stable operating temperature of the DPMVM is 66.1 °, which is 6.8° lower than the simulated one. It can be found that even though the estimated efficiency is close to the experimental one, which means the estimated loss is close to the actual loss, the error between the temperature rise is a little large. This error is mainly caused by the estimation error of the copper loss. The estimated copper loss is 113.4 W. However, the phase resistor of the prototype is 1.5 Ω (at 27.3 °), and the actual input current is 3.4 A. Therefore, the copper loss under the stable operating temperature (66.1 °) should be 78.4 W. The thermistors are set at the end of armature winding, and the heat exchange of winding is poor in the motor. What's more, copper loss is the main heat source in the DPMVM. Thus, the temperature rise estimation error is large.

VI. CONCLUSION

Conventional SMPMMs in direct-drive applications suffer bulky size and low-efficiency problems. To solve this problem, in a direct-drive industrial turbine application, a low-cost high-efficiency DPMVM with rectangular and trapezoidal PMs is designed and optimized to replace the SMPMM. The topology of it is carefully selected based on recent studies, as well as the slot/pole combination of it. And the design parameters of the DPMVM is optimized according to the sensitivity analysis results. A final design of DPMVM is obtained by modifying the shapes of stator and rotor PMs to trapezoidal and rectangular. The cost of PMs is reduced by 17.7%, and the performance of the DPMVM is almost kept the same.

Besides the initial SMPMM with 24 stator slots, the other typical SMPMM with the same rotor pole pairs as the DPMVM is also selected for comparison. The results show that the efficiency of the DPMVM is 12% higher than the 24SMPMM experimentally and 6.5% higher than the 72SMPMM given simulation. Moreover, the material cost of the DPMVM is the lowest. The cost of DPMVM is 6.87% cheaper than 24SMPMM and 16.65% cheaper than 72SMPMM. The performance of the DPMVM is validated by experiment. It shows that the DPMVM is a competitive candidate for industrial turbine applications.

REFERENCES

[1] W. Chlebosz, G. Ombach, and J. Junak, "Comparison of permanent magnet brushless motor with outer and inner rotor used in e-bike," in *Proc. XIX Int. Conf. Electr. Mach. (ICEM)*, Rome, Italy, Sep. 2010, pp. 1–5.

[2] S. Chi, Z. Zhang, and L. Xu, "Sliding-mode sensorless control of direct-drive PM synchronous motors for washing machine applications," *IEEE Trans. Ind. Appl.*, vol. 45, no. 2, pp. 582–590, Apr. 2009, doi: 10.1109/TIA.2009.2013545.

[3] K. T. Chau, Y. B. Li, J. Z. Jiang, and S. Niu, "Design and control of a PM brushless hybrid generator for wind power application," *IEEE Trans. Magn.*, vol. 42, no. 10, pp. 3497–3499, Oct. 2006, doi: 10.1109/TMAG.2006.879436.

[4] D.-K. Hong, J.-Y. Lee, B.-C. Woo, D.-H. Park, and B.-U. Nam, "Investigating a direct-drive PM type synchronous machine for turret application using optimization," *IEEE Trans. Magn.*, vol. 48, no. 11, pp. 4491–4494, Nov. 2012, doi: 10.1109/TMAG.2012.2199096.

[5] S.-I. Kim, J. Cho, S. Park, T. Park, and S. Lim, "Characteristics comparison of a conventional and modified spoke-type ferrite magnet motor for traction drives of low-speed electric vehicles," *IEEE Trans. Ind. Appl.*, vol. 49, no. 6, pp. 2516–2523, Nov. 2013, doi: 10.1109/TIA.2013.2264651.

[6] Y. Yang, M. M. Rahman, T. Lambert, B. Bilgin, and A. Emadi, "Development of an external rotor V-shape permanent magnet machine for E-bike application," *IEEE Trans. Energy Convers.*, vol. 33, no. 4, pp. 1650–1658, Dec. 2018.

[7] J. Zhang, B. Zhang, G. Feng, and B. Gan, "Design and analysis of a low-speed and high-torque dual-stator permanent magnet motor with inner enhanced torque," *IEEE Access*, vol. 8, pp. 182984–182995, 2020, doi: 10.1109/ACCESS.2020.3028425.

[8] Y. Liu, L. Li, Q. Gao, J. Cao, and Z. Sun, "An analytical model and optimization of a novel hybrid rotor machine for high torque density," *IEEE Trans. Energy Convers.*, vol. 36, no. 1, pp. 230–241, Mar. 2021, doi: 10.1109/TEC.2020.3008768.

[9] S. L. Ho, S. Niu, and W. N. Fu, "Design and comparison of Vernier permanent magnet machines," *IEEE Trans. Magn.*, vol. 47, no. 10, pp. 3280–3283, Oct. 2011, doi: 10.1109/TMAG.2011.2157309.

[10] F. Wu and A. M. El-Refaie, "Permanent magnet Vernier machine: A review," *IET Electric Power Appl.*, vol. 13, no. 2, pp. 127–137, Feb. 2019.

[11] D. Li, R. Qu, J. Li, and W. Xu, "Design of consequent pole, toroidal winding, outer rotor Vernier permanent magnet machines," in *Proc. IEEE Energy Convers. Congr. Exposit. (ECCE)*, Sep. 2014, pp. 2342–2349, doi: 10.1109/ECCE.2014.6953716.

[12] Y. Gao, R. Qu, D. Li, J. Li, and G. Zhou, "Consequent-pole flux-reversal permanent-magnet machine for electric vehicle propulsion," *IEEE Trans. Appl. Supercond.*, vol. 26, no. 4, pp. 1–5, Jun. 2016.

[13] X. Zhao and S. Niu, "A new slot-PM Vernier reluctance machine with enhanced zero-sequence current excitation for electric vehicle propulsion," *IEEE Trans. Ind. Electron.*, vol. 67, no. 5, pp. 3528–3539, May 2020.

[14] X. Zhao, S. Niu, X. Zhang, and W. Fu, "Design of a new relieving-DC-saturation hybrid reluctance machine for fault-tolerant in-wheel direct drive," *IEEE Trans. Ind. Electron.*, vol. 67, no. 11, pp. 9571–9581, Nov. 2020, doi: 10.1109/TIE.2019.2955418.

[15] A. Toba and T. A. Lipo, "Generic torque-maximizing design methodology of surface permanent-magnet Vernier machine," *IEEE Trans. Ind. Appl.*, vol. 36, no. 6, pp. 1539–1546, Nov. 2000.

[16] D. Li, R. Qu, and T. Lipo, "High-power-factor Vernier permanent-magnet machines," *IEEE Trans. Ind. Appl.*, vol. 50, no. 6, pp. 3664–3674, Nov./Dec. 2014.

[17] D. Li, R. Qu, J. Li, and W. Xu, "Consequent-pole toroidal-winding outer-rotor Vernier permanent-magnet machines," *IEEE Trans. Ind. Appl.*, vol. 51, no. 6, pp. 4470–4481, Nov./Dec. 2015.

[18] L. Wu, R. Qu, D. Li, and Y. Gao, "Influence of pole ratio and winding pole numbers on performance and optimal design parameters of surface permanent-magnet Vernier machines," *IEEE Trans. Ind. Appl.*, vol. 51, no. 5, pp. 3707–3715, Sep./Oct. 2015.

[19] A. Ishizaki, "Theory and optimum design of PM Vernier motor," in *Proc. 7th Int. Conf. Electr. Mach. Drives*, Durham, U.K.,1995, pp. 208–212.

[20] K. Xie, D. Li, R. Qu, and Y. Gao, "A novel permanent magnet Vernier machine with Halbach array magnets in stator slot opening," *IEEE Trans. Magn.*, vol. 53, no. 6, pp. 1–5, Jun. 2017.

[21] R. Ishikawa, K. Sato, S. Shimomura, and R. Nishimura, "Design of in-wheel permanent magnet Vernier machine to reduce the armature current density," in *Proc. Int. Conf. Electr. Mach. Syst. (ICEMS)*, Busan, South Korea, Oct. 2013, pp. 459–464, doi: 10.1109/ICEMS.2013.6754567.

[22] S. Niu, T. Sheng, X. Zhao, and X. Zhang, "Operation principle and torque component quantification of short-pitched flux-bidirectional-modulation machine," *IEEE Access*, vol. 7, pp. 136676–136685, 2019.

[23] Y. Gao and M. Doppelbauer, "Comparative analysis of double flux modulation flux reversal machines with PMs on both stator and rotor," in *Proc. Int. Conf. Electr. Mach. (ICEM)*, Aug. 2020, pp. 1964–1970, doi: 10.1109/ICEM49940.2020.9270884.

[24] H. Yang, Y. Li, H. Lin, W. Liu, and X. Zhao, "Novel dual-sided permanent magnet machines with different stator magnet arrangements," in *Proc. IEEE Energy Convers. Congr. Exposit. (ECCE)*, Baltimore, MD, USA, Sep. 2019, pp. 6114–6121, doi: 10.1109/ECCE.2019.8913247.

[25] X. Zhao, S. Niu, X. Zhang, and W. Fu, "A new relieving-DC-saturation hybrid excitation Vernier machine for HEV starter generator application," *IEEE Trans. Ind. Electron.*, vol. 67, no. 8, pp. 6342–6353, Aug. 2020.

[26] Y. Shi, T. W. Ching, L. Jian, and W. Li, "A new dual-permanent-magnet-excited motor with hybrid stator configuration for direct-drive applications," in *Proc. 22nd Int. Conf. Electr. Mach. Syst. (ICEMS)*, Aug. 2019, pp. 1–6, doi: 10.1109/ICEMS.2019.8921452.

[27] Z. Liang, Y. Gao, D. Li, and R. Qu, "Design of a novel dual flux modulation machine with consequent-pole spoke-array permanent magnets in both stator and rotor," *CES Trans. Elect. Mach. Syst.*, vol. 2, no. 1, pp. 73–81, Mar. 2018, doi: 10.23919/TEMS.2018.8326453.

[28] L. Xu, W. Zhao, M. Wu, and J. Ji, "Investigation of slot–pole combination of dual-permanent-magnet-excited Vernier machines by using air-gap field modulation theory," *IEEE Trans. Transport. Electrific.*, vol. 5, no. 4, pp. 1360–1369, Dec. 2019.

[29] C. Gong and F. Deng, "Design and optimization of a high-torque-density low-torque-ripple Vernier machine using ferrite magnets for direct-drive applications," *IEEE Trans. Ind. Electron.*, vol. 69, no. 6, pp. 5421–5431, Jun. 2022, doi: 10.1109/TIE.2021.3090714.

[30] Q. Lin, S. Niu, F. Cai, W. Fu, and L. Shang, "Design and optimization of a novel dual-PM machine for electric vehicle applications," *IEEE Trans. Veh. Technol.*, vol. 69, no. 12, pp. 14391–14400, Dec. 2020, doi: 10.1109/TVT.2020.3034573.

QIFANG LIN received the Ph.D. degree from the Department of Electrical Engineering, The Hong Kong Polytechnic University, Hong Kong, China, in 2021. She is currently an Associate Professor at the College of Information Science and Engineering, Huaqiao University. Her research interests include electrical machine and renewable energy conversion.

XING ZHAO (Member, IEEE) received the B.Eng. degree in electrical engineering from the Nanjing University of Aeronautics and Astronautics, Nanjing, China, in 2014, and the Ph.D. degree in electrical engineering from The Hong Kong Polytechnic University, Hong Kong, in 2020.

From July 2019 to January 2020, he was a Visiting Research Scholar with the Center for Advanced Power Systems, Florida State University, Tallahassee, FL, USA. From July 2020 to October 2021, he worked as a Research Assistant Professor with the Department of Electrical Engineering, The Hong Kong Polytechnic University. Since November 2021, he has been a Lecturer with the Department of Electronic Engineering, University of York, York, U.K. He has authored or coauthored more than 50 technical papers in the international journals and conferences and holds six granted patents. His research interests include advanced electrical machines, motor drives, power electronics for electric vehicles, and renewable energy systems.

FENGBIN CAI received the B.Sc. degree in electrical engineering from Xiamen University, Xiamen, China, in 2018. He is currently a Research and Development Manager at the Research and Development Center for Rare Earth Materials and Applications, Xiamen Tungsten Company Ltd., Xiamen. His main research interests include electrical machine design, optimization, and machine drive.

QIANNAN WU received the B.Sc. degree in electrical engineering from Huaqiao University, Xiamen, China, in 2019. She is currently an Electromagnetic Design Engineer with the Research and Development Center for Rare Earth Materials and Applications, Xiamen Tungsten Company Ltd., Xiamen. Her main research interests include electrical machine design and optimization.

JIAPENG PANG received the master's degree in electrical engineering from Huaqiao University. His current research interests include electrical machine and renewable energy conversion.

XINHUA GUO received the M.S. degree in agricultural electrification and automation from Jiangsu University, Zhenjiang, China, in 2006, and the Ph.D. degree in electrical engineering from the Institute of Electrical Engineering (IEE), Chinese Academy of Sciences (CAS), Beijing, China, in 2010. He is currently working as a Professor and the Deputy Dean of the College of Information Science and Engineering, Huaqiao University, Xiamen, China. In additional, he was a Research Assistant at IEE, CAS, and worked as an Engineer at Japanese Company TDK and American Company Amphenol Assemble Tech (Xiamen) Company Ltd. His current research interests include IGBT packaging technology, PMSMs and their drive control for EVs, and special motors and their drive control.

• • •